Electromagnetic Redesign of NASA's High Efficiency Megawatt Motor

Thomas T. Tallerico[1] and Justin J. Scheidler[2]

NASA Glenn Research Center, Cleveland, OH, 44135, USA

Dongsu Lee[3] and Kiruba Haran[4]

University of Illinois at Urbana-Champaign, Urbana, IL, 61801, USA

NASA's High Efficiency Megawatt Motor (HEMM) is being developed to achieve the performance needed by single aisle class electrified aircraft. It is a 1.4 MW electric machine designed as a generator for NASA's STARC-ABL concept vehicle. It has performance objectives of greater than 16 kW/kg electromagnetic specific power and efficiency of greater than 98%. A significant flaw in the preliminary electromagnetic design of HEMM was recently discovered. The stator teeth in the preliminary design cause the magnetic flux in the rotating components of HEMM to oscillate at a very high frequency (12,240 Hz). Two independent energy loss analyses are presented to show that the frequency is high enough to cause eddy current losses that significantly exceed the rotor's loss limit (50 W), despite the very small magnitude of this flux oscillation (<0.01 T). To eliminate these rotor losses, while continuing to meet the target performance, it was determined that the stator teeth needed to be removed and the electromagnetic geometry of the motor needed to be revised. The revised, slotless HEMM motor design is summarized. Sensitivity of the new design to key unknown variables such as the temperature of and number of turns in the superconducting rotor coils and the stator winding's average temperature.

I. Nomenclature

A	=	*Area*	w	=	tangential width of a component
B	=	magnetic flux density	V	=	volume
d	=	wire diameter	α	=	Stienmetz frequency coefficient
l	=	axial length of component	β	=	Stienmetz flux density coefficient
L	=	overall length	γ	=	Stienmetz Coefficient
M	=	Mass	γ_1	=	Modified Stienmetz Coefficient
P	=	power loss	ρ	=	resistivity
t	=	time			
T	=	time period of magnetic flux repetition			

II. Introduction

In order to enable electrified aircraft, high performance electric machines need to be developed with increased efficiency and specific power. NASA's High Efficiency Megawatt Motor (HEMM) is a 1.4 megawatt wound-field synchronous machine being developed at NASA's Glenn Research Center to achieve the required performance of electrified aircraft. HEMM is designed to meet the requirements of the two generators on NASA's STARC-ABL concept aircraft [1]. It has performance targets of greater than 16 kW/kg electromagnetic specific power and greater

---
[1] Research Engineer, Rotating and Drive Systems Branch, thomas.tallerico@nasa.gov.
[2] Research Mechanical Engineer, Rotating and Drive Systems Branch, justin.j.scheidler@nasa.gov.
[3] Post doc, Department of Electrical and Computer Engineering, dongsul@illinois.edu .
[4] Associate Professor, Department of Electrical and Computer Engineering, kharan@illinois.edu.

than 98% efficiency. These high performance targets are primarily achieved through the use of a self-cooled high temperature superconducting rotor.

The preliminary design of HEMM has been discussed in a number of publications [2] [3] [4] [5]. In the preliminary design, a semi-slotless stator was selected to create a mechanical torque transmission path and improve thermal conductivity between the stator windings and the stator back iron. A semi-slotless design was permitted, because initial analysis of the motor using off the shelf motor analysis tools showed no significant rotor magnetic loss. Recently, higher fidelity efficiency analysis of this motor was completed. The analysis indicates a flaw in the original analysis as it predicts very significant rotor losses that exceed the thermal capacity of HEMM's cryocooler (≤ 60 W rejection at 50 K). A redesign of HEMM with a slotless stator was therefore required.

This paper presents the higher fidelity energy loss analysis of the preliminary design (Section III), a verification of the excessive eddy current loss in the rotor using an alternative modeling approach (Section IV), a summary of the selected updated design for HEMM (Section V), and the sensitivity of the updated design's efficiency to key uncertainties in the manufacturing and performance of the machine (Section VI).

III.   Refined Energy Loss Analysis of HEMM's Preliminary Design

This section details the higher fidelity energy loss analysis of HEMM's preliminary design. The preliminary design is first summarized (Section III-A), and then the analysis methodology is described (Section III-B). Lastly, the predicted energy loss is discussed (Section III-C).

A. Summary of the Preliminary Design

A single pole of the electromagnetic preliminary design of HEMM and its rotor structure are depicted in Figure 1. The stator is a 9 phase, semi-slotless, wound-field design. Its geometry is quantified in Ref [3] and summarized below in Table 1. The stator is referred to as semi-slotless, because the stator teeth between each of the 108 coil slots are only wide enough to handle a small portion of the total flux produced by the rotor. The bulk of the flux in the motor therefore behaves as if the motor is slotless. The stator teeth were added to the preliminary design originally to create a mechanical torque transmission path and improve the thermal conductivity between the stator windings and the stator back iron. They also were found to provide a non-trivial increase in the design's torque relative to a slotless design. However, as will be shown in the following sections, these stator teeth created spatial variations in the magnetic permeability of the stator that resulted in time varying flux and therefore magnetic loss in the rotor.

The preliminary design's rotor has 12 poles composed of 2nd generation high temperature superconductor. The rotor back iron is made of $Fe_{49.15}Co_{48.75}V_2$. The nominal design speed of the rotor is 6,800 rpm. The superconducting coils

Figure 1: Preliminary electromagnetic and structural design of HEMM (stator coils not shown).

have a so-called 'no-insulation' topology where the conductors are wound with no additional insulation or epoxy between turns. The non-superconducting layers of the superconducting tape act as the turn-to-turn insulation for the coil. This coil topology improves reliability by both reducing the possibility of tensile stresses being transmitted through the thickness of the conductor, and creating a high conductivity path for current to flow turn-to-turn in the event that a given area of the coil becomes non-superconducting temporarily. The downside to this topology is that
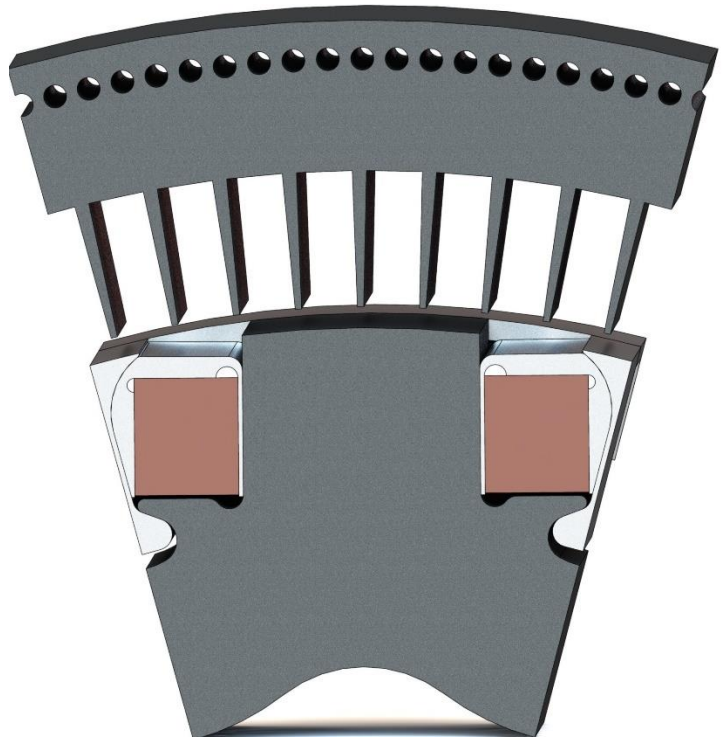
the low turn-to-turn resistance, both makes eddy currents in the rotor more significant, and makes modeling the flow path of eddy currents in the coil difficult to predict. Table 1 summarizes the geometry of the preliminary motor design.

Table 1 Specifications of the preliminary design of HEMM's stator

Stator			
Stator Windings		**Stator Core**	
Number of Phases	9	Back Iron ID	345 mm
Number of Poles	12	Back Iron OD	383 mm
Layout	Lap, 2 Layer, Over/under	Stack Length	125 mm
Litz wire	8x8 mm, 6000x40 AWG	Slots	108
Wire Material	Copper	Slot Width	8 mm
Winding OD	345 mm	Slot Depth	19.5 mm
Winding ID	313 mm	Material	$Fe_{49.15}Co_{48.75}V_2$
Stator Winding Mass	17.96 Kg	Stator Core Mass	21.5 Kg

Table 2: Specifications of the preliminary design of HEMM's rotor

Rotor		Coil	
Type	DC wound Field	Number of Layers	4
Number of Rotor Poles	12	Number of Turns per Layer	229
Operating Temp	<62.5 K	Coil Width	14.9 mm
		Coil Height	16.75 mm
Rotor Core		Coil Fill Assumed	100%
Outer Diameter	300 mm	Conductor Height	4 mm
Stack Length	125 mm	Conductor Width	65 um
Tooth Width	34 mm	Material	REBCO
Tooth Height	24.2 mm	Operating Current	51.5
Back Iron Thickness	25.4 mm	Total Cost Superconductor (assuming $60/m)	$272k
Material	$Fe_{49.15}Co_{48.75}V_2$		
Mass	30 kg	Total Mass Superconductor	7 kg

B. Energy Loss Analysis Methodology

Electromagnetic efficiency analysis was carried out using a collection of 2D static FEA simulations to estimate the torque and the magnitude of the time varying magnetic field in HEMM's magnetic components. For the analysis presented here, 181 static simulations were run over $1/6^{th}$ of a rotor rotation (10 points per stator tooth passage over one electrical period). Magnetic flux density magnitude vs rotor position and torque data were abstracted from the FEA and post processed using analytical equations to create loss predictions. Using this analysis methodology the losses are potentially over estimated as the bidirectional coupling of the magnetic field and the eddy currents in the magnetic components is neglected. When the eddy currents in a machine are of low enough magnitude, as is the case in most high efficiency machines, the over estimation is negligible. In the analysis presented here, that is not the case and the loss over prediction in the HEMM preliminary design's rotor is not negligible. The accuracy of the exact loss values presented here are therefore questionable, but they are sufficient to show that the rotor losses in the preliminary design would have exceeded the 50 Watt limit of HEMM's cryocooler. An example snap shot of the magnetic field in one of the static simulations is shown in Figure 2. The methodologies used to predict each loss are summarized in the following sections.
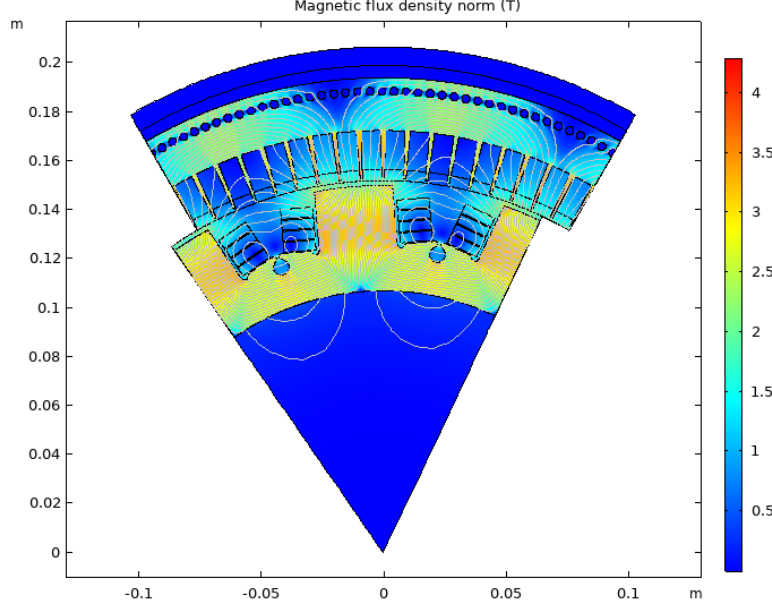
Figure 2: Example Static Magnetic Finite Element Simulation Used to Quantify the Magnetic Flux Density Variation in Each Component.

1. Stator Winding Resistive Loss

Resistive losses in the stator windings were predicted using:

$$Loss_{I2R} = \frac{\rho_{litz} * L_{litz} * I_{rms}^2}{A_{litz}} \tag{1}$$

Where $Loss_{I2R}$ are the stator resistive losses, ρ_{litz} effective resistivity of the litz wire accounting for AC effects, L_{litz} is the total length of litz wire in the stator, A_{litz} is the copper area in a single 8x8 mm litz wire bundle. ρ_{litz} is calculated at a temperature of 135C. AC resistivity is assumed to be zero since the diameter of the 40 AWG wire in the litz bundle is much less than the skin depth for copper at the HEMM's electrical operating frequency. L_{litz} is taken to be 69.31 m (42.31 m of end windings + 108*2*.125m of active axial length). I_{rms} was set at 450 Amps to achieve the desired output torque.

2. Stator Iron Loss

Stator iron loss were predicted using the improved generalized Steinmetz equation [6]:

$$P_v = \frac{1}{T} \int_0^T \gamma_1 \left| \frac{dB}{dt} \right|^\alpha (\Delta B)^{\beta - \alpha} dt \tag{2}$$

$$\gamma_1 = \frac{\gamma}{2^{\beta - 1} \pi^{\alpha - 1} \int_0^{2\pi} |\cos(\theta)|^\alpha d\theta} \tag{3}$$

Where P_v is volumetric loss density, T is the period of repetition of the field, B is magnetic flux density, t is time, ΔB is the peak to peak flux density, and k_1 is an updated loss coefficient. α, β, and k are the standard Steinmetz loss coefficients.

3. Stator Winding Proximity Loss

Winding Proximity Losses are modeled using the common proximity loss equation for round conductors in a magnetic field.

$$Loss_{proximity} = \frac{1}{12} \frac{V}{\rho} d^2 \frac{1}{T} \int_0^T \left(\frac{dB}{dt} \right)^2 dt \tag{4}$$

Where $Loss_{proximity}$ is the proximity loss in a conductor, V is the volume of the conductor in the magnetic field, ρ is the conductors resistivity, and d is the diameter of the wire.

4. Rotor Iron Loss

The only losses in the rotor iron are assumed to be traditional eddy currents since the rotor coils fully saturate the rotor iron. All variations in field occur at levels above saturation and therefor the rotor iron can be treated as a non-soft

magnetic material. Since the rotor iron is un-laminated and all the time varying flux is assumed to occur in the rotor teeth the eddy current losses in the rotor are modeled using the equations for eddy current losses in rectangular magnets [7]

$$P_{eddy} = \frac{1}{16}\frac{V}{\rho}\frac{w^2 l^2}{w^2+l}\frac{1}{T}\int_0^T (\frac{dB}{dt})^2 \, dt \qquad (5)$$

Where P_{eddy} is the eddy current power loss, w the tangential width of the magnet, l is the axial length of a given magnet section, V is the volume of the magnet, ρ is the resistivity of the material, T is the period of repetition, and B is magnetic field magnitude. For the rotor iron *w* is taken to be the rotor tooth width and *l* is set to the rotor stack length.

It is important to note that at nominal operating speed (6800 rpm) the stator tooth pass frequency relative to the rotor is 12,240 Hz. At this frequency, the skin depth in $Fe_{49.15}Co_{48.75}V_2$ is 3 mm. The bulk of the time varying flux in the rotor iron is at this frequency and therefore the eddy currents in the rotor would be skin depth limited instead or resistance limited. Therefore Equation 5 potentially overestimate loss, but at the time of writing this paper no suitable and validated model for skin depth limited eddy currents could be found.

5. Rotor Titanium Structure Eddy Current Loss
Time varying field in the rotor's structural titanium components was also observed in the finite element analysis. Similar to the rotor iron, the time varying field occurred mostly at the farthest radially outward portions of the rotor iron. The loss in these components was estimated using Equation 5 as well. For the titanium, *w* was taken to be the width of the cup (16 mm) and *l* was taken to be the stack length (125 mm). Titanium has a skin depth of ~3 mm at 12,240 Hz and therefore its loss also will be potentially overestimated by Equation 5.

6. Superconductor Proximity Loss
Time varying field was also observed in the superconducting coil in the efficiency analysis. How the eddy currents would flow in the superconducting coil and what the effective bulk resistance of the coil to eddy currents would be is questionable given that it is essentially a composite structure that has no insulation between turns of superconductor. As an approximation to quantify the possibility of losses and not in any attempt to quantify the exact value, Equation 5 was applied assuming the coil is a solid rectangular block of copper. *w* was taken to be the width of the coil (14.95 mm) and *l* was taken to be the stack length (125 mm).

C. Energy Loss Predictions
The results of the loss calculation are shown in Table 3 below. Stator losses come back as expected relative to previous analysis of the preliminary HEMM design. Rotor losses comeback well above the original expectation of <60 Watts. Note that as discussed above the rotor loss estimates, especially the superconductor eddy loss estimate, are not expected to be wholly accurate, but more representative of the possible loss. Regardless, the estimated rotor losses are orders of magnitude greater than the <60 Watts that HEMM's cryocooler can reject at an operating temperature of 50 K and therefore the HEMM preliminary design would not have worked.

Table 3: Predicted energy losses in HEMM's preliminary design.

Stator Losses		Rotor Losses	
Resistive Loss	11,816 W	Iron Eddy Loss	19.6 kW
Proximity Loss	157 W	Titanium Eddy Loss	12.5 kW
Iron Loss	6648 W	Superconductor Eddy Loss	108 kW

Figure 3a shows an example magnetic wave form vs rotor position in the rotor iron from the efficiency analysis. The frequency of the waveform exactly matches the stator slot passage frequency relative to the rotor. To show that the stator teeth were the cause of the time varying rotor flux, the analysis was rerun without stator teeth. Figure 3b shows the flux vs rotor position without stator teeth at the same point in the rotor as 3a. No notable time varying flux is observed. A redesign of the HEMM stator to remove or reduce the effect of the stator teeth was therefore required.
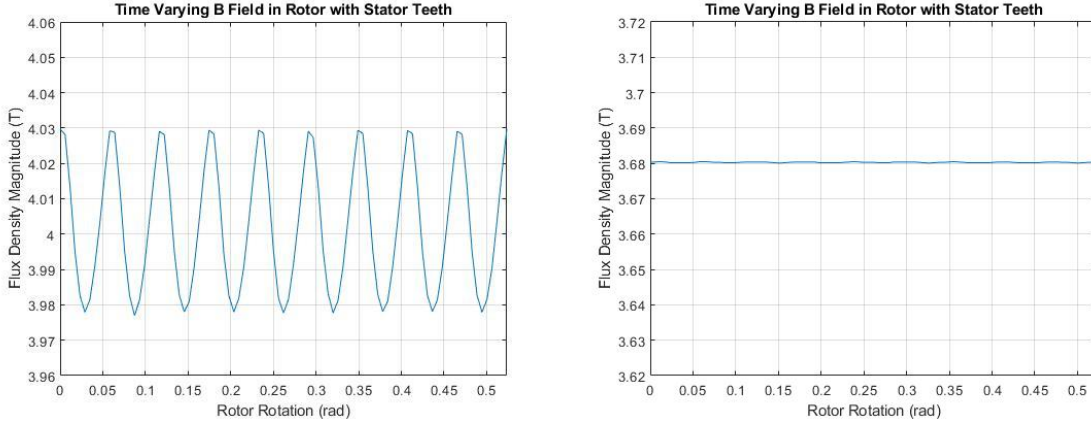
Figure 3: Example magnetic flux density variation in the rotor (a) with and (b) without stator teeth.

IV. Verification of the Energy Loss in the Rotor of HEMM's Preliminary Design

An independent evaluation of the rotor core loss for HEMM was used to verify that the methodology described in section III was not giving misleading results. This independent analysis used time varying FEA and careful analysis of mesh and time step resolution. The analysis both verifies the results in Section III and points to why the rotor losses were initially missed in the preliminary design of HEMM.

A. Description of the Model

A 2D transient finite element simulation was used to verify the eddy current loss in the rotor iron only. This alternative model includes full coupling between the electric and magnetic potentials (i.e., the eddy currents induced in the solid domains oppose and reduce the changes in magnetic flux). The transient analysis was conducted for three different meshes and four different time step sizes that correspond to rotor angle changes of 10, 1, 0.1, and 0.01 mechnical degrees. In each case, the simulation was run for one electrical period (60 mechanical degrees), as shown in Figure 4.
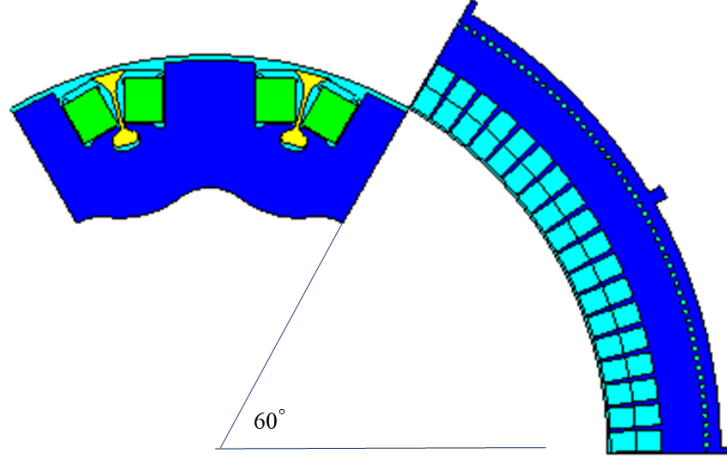

Figure 4: 2D transient finite element model used to verify the eddy current loss in the rotor of HEMM's preliminary design.

B. Rotor Energy Loss Results

The spatial distribution of the eddy current loss in the rotor at a single time step is shown in Figure 5. In the rotor iron, the eddy currents are highly concentrated at the top of each rotor tooth near the tips of the stator teeth. Figure 6 depicts the dependence of the total eddy current loss prediction on the size of the time step used in the analysis in terms of mechanical degrees.
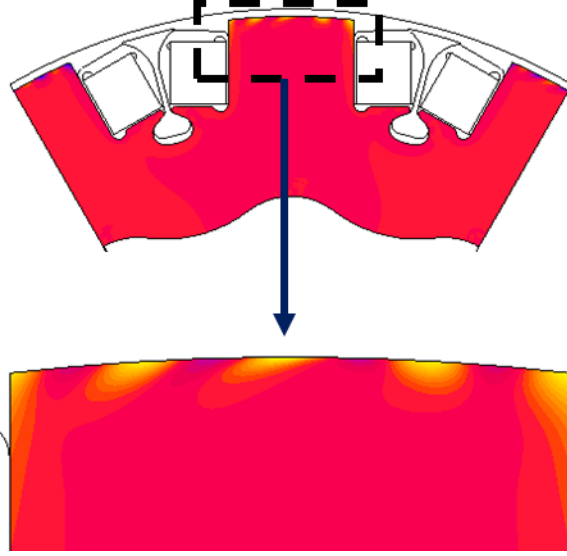
Figure 5: Spatial distribution of the eddy current loss in the rotor iron at a given point in time calculated by a 2D transient finite element model (results shown for case of 163,005 mesh elements).
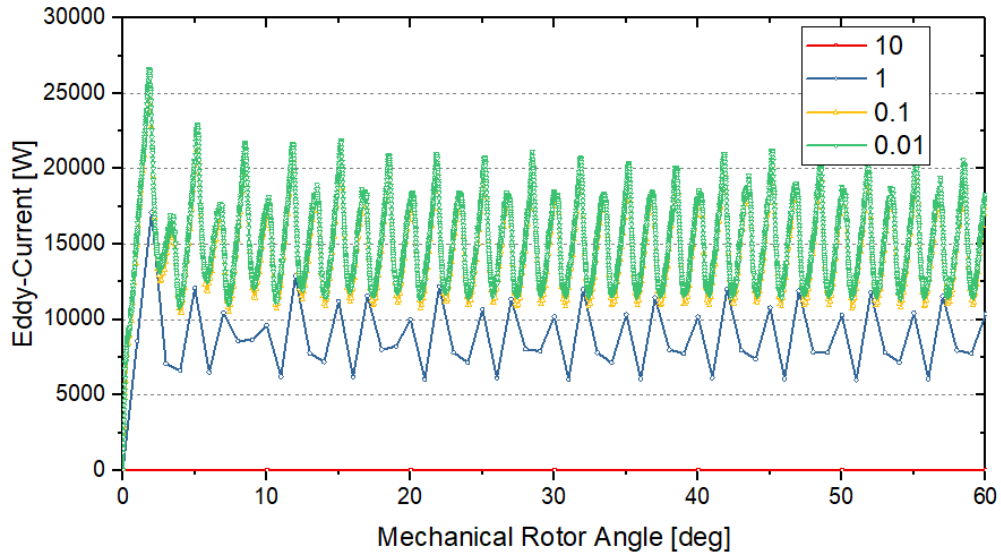

Figure 6: Time dependence of the total eddy current loss in the rotor iron for four different mechanical angle steps.

The time-averaged total eddy current loss in the rotor back iron is summarized in Table 4 for all the different combinations of mesh resolution and time step size used in this analysis. The results show little dependence on mesh resolution. They do however show significant dependence on the size of the time step used. This dependence potentially points to why this loss was initially missed by the commercial tool used to complete the preliminary design of HEMM.

The rotor back iron loss predicted by the alternative energy loss model (15.3 kW) is less than that predicted by the energy loss model in Section III (19.6 kW). The discrepancy is believed to result from the neglecting of bidirectional coupling with this large of an eddy current loss. Even if one or both of these predictions has considerable error, they clearly indicate that the preliminary design of HEMM has a total amount of rotor eddy current losses that significantly exceeds the 50 W limit the HEMM cryocooler. Consequently, an electromagnetic redesign of HEMM was required to ensure that it can function as intended.

7

Table 4: Rotor iron eddy current loss calculated by a 2D transient finite element model.

Number of mesh elements	Change in mechanical angle between subsequent time steps			
	10°	1°	0.1°	0.01°
31,976	1 W	9,132 W	14,940 W	15,630 W
59,556	1 W	8,754 W	14,532 W	15,228 W
163,005	1 W	8,760 W	14,532 W	15,282 W

V.   Updated HEMM Design with Acceptable Level of Rotor Energy Loss

Various design options were considered for eliminating the eddy current loss in the rotor. Design options considered included an eddy current shield, laminated rotor core, and reduced stator tooth height. An eddy current shield on the rotor would be difficult to implement, because it couldn't be connected directly to the cryogenic rotor without still exceeding the cryocooler heat rejection limit. Integrating a shield such that it was connected to the rotor shaft but not the cryogenic parts of the rotor would have required a complicated structure and a significant increase in the airgap of the machine that was deemed unacceptable.

Laminating the rotor iron would only serve to suppress the rotor iron loss in the machine. The super conducting coils and structure would still have significant loss. Moving the coils and their structures radially inward and away from the stator teeth with a laminated core was examined, but this resulted in both a larger effective airgap for the conductor once the rotor iron is saturated and the loss of magnetic material due to geometric constraints.

Reducing the stator tooth height did lead to significant reductions in all eddy current losses; however, the loss reductions were not sufficient to reduce rotor losses to below the cryocooler heat rejection limit unless the teeth were eliminated entirely. The simple removal of the stator teeth from the preliminary design of HEMM would result in a ~200 Nm reduction in torque. A ~10% increase in stator current and a corresponding 21% increase in the stator windings' resistive losses would have been required to achieve the target torque and power of HEMM. This increase would have resulted in a nominally 98.24% efficient machine which is still above the target 98% efficiency. However, at this point in the design process for HEMM a 20% margin is being held on the machine's total losses. With this margin included that machines efficiency drops 97.89% efficiency. This was deemed to be unacceptable and a highly constrained redesign was performed.

To complete the redesign, a design tool for the HEMM topology was developed. This tool uses parametric sweeps of various motor geometry parameters, rotor current, and stator current in a static electromagnetic FEA model to create predictions for the rotor coil's critical current, stator losses, total machine mass, and STARC-ABL fuel burn. The full details of this tool are out of the scope of this paper and the subject of a future publication.

For the redesign, the tool was constrained to use the same litz wire in the stator and the stator winding geometry from the preliminary HEMM design, because of the heavy investment already made into figuring out how to manufacture those stator windings. The stack length of the machine was limited to 150 mm due to the available size of $Fe_{49.15}Co_{48.75}V_2$ billets to make the rotor out of. Total superconductor cost was limited to $200k. Parametric sweeps of stator back iron thickness, rotor back iron thickness, and rotor tooth width were then carried out and a design was selected based on the target HEMM specifications and the predicted impact on STARC ABL fuel burn.

The design parameters for the selected design are listed in Table 5. Figure 7 shows the updated electromagnetic geometry for HEMM. Table 6 presents the results of an efficiency analysis of this new electromagnetic geometry using the methodology described in Section III. Table 7 shows the rotor losses predicted by that analysis in order to show that the rotor loss has been eliminated with the redesign of the motor.

Table 5: Summary of specifications for the updated design of HEMM.

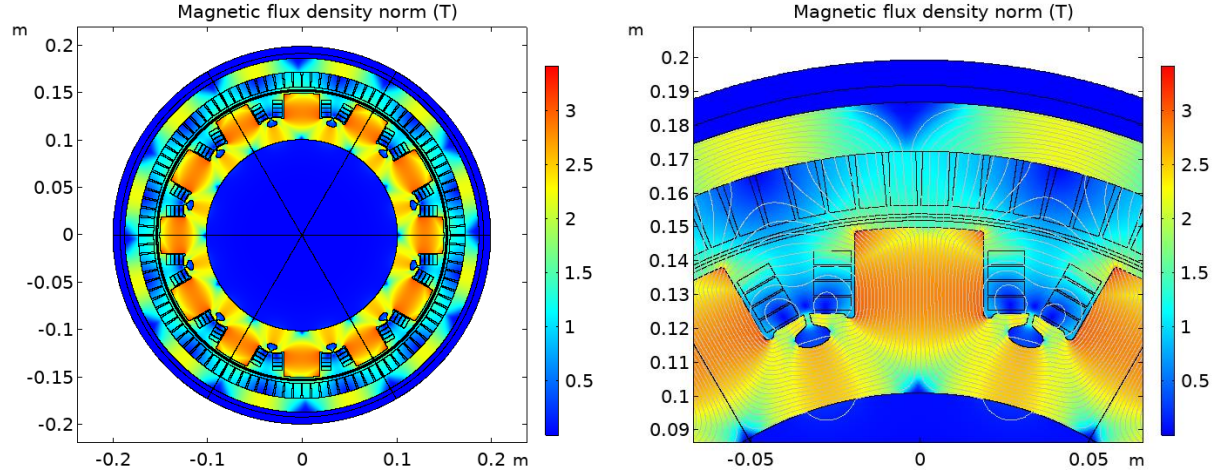| Stator		Rotor			
		Iron		Coil	
Type	Slotless	Stack Length	150 mm	Number of Layers	4
Back Iron Outer Diameter	374 mm	Outer Diameter	300 mm	Number of Turns per Layer	150
Back Iron Inner Diameter	345 mm	Inner Diameter	~200 mm	Coil Width	10.833
Winding Inner Diameter	313 mm	Tooth Width	38 mm	Coil Height	18 mm
Wire	8x8 mm Litz wire 3000 strands (40 AWG)	Tooth Height	~25 mm	Coil Fill Factor	90%
		Back Iron Thickness	~20 mm	Conductor Height	4 mm
Stack Length	150 mm	Mass	34.7 kg	Conductor Width	65 um
Stator Winding Length	74.71 m			Material	REBCO
Skew	0			Operating Current	57.2 A
Stator Iron Mass	19.95 kg			Total Cost Superconductor (est.)	$200k
Stator Winding Mass	19.36			Total Mass Superconductor	7 kg

Figure 7 Geometry of Updated HEMM Electromagnetic Design

Table 6: Predicted energy losses and efficiency of the updated HEMM design.

	No Margin (Watts)	20% Margin (Watts)
Resistive Losses	10981	13177
Winding Proximity Loss	41	49
Iron Loss	4558	5469
Total Stator Loss	15580	18696
Total Rotor Loss	2	2
Other Losses	4000	4800
Total Losses	19580	23496
Efficiency	98.61%	98.33%

Table 7 Rotor Loss Esimates for Electromagnetic Redesign of HEMM

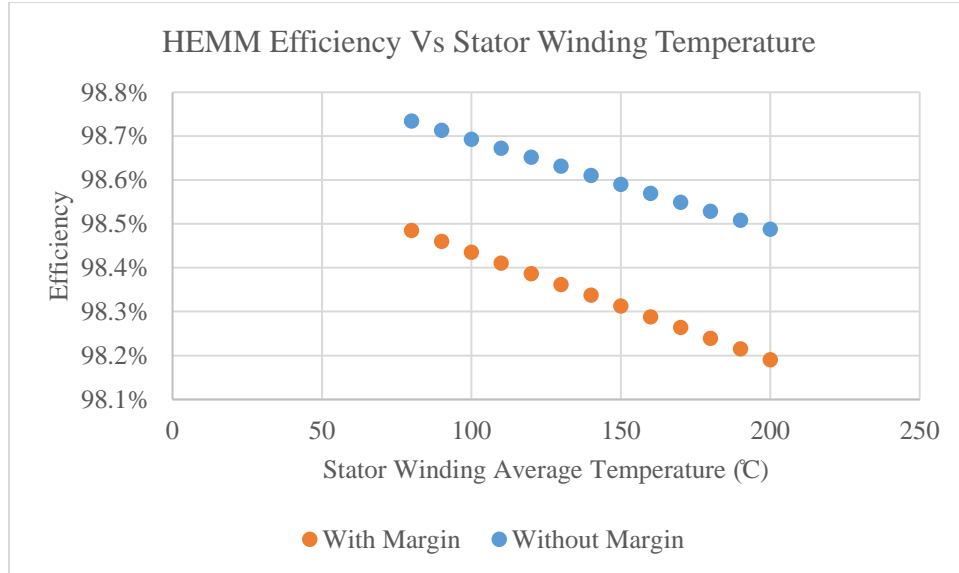| Rotor Loss Predictions	
Iron Eddy Loss	0.6 W
Titanium Eddy Loss	0.5 W
Superconductor Eddy Loss	0.95 W

The updated electromagnetic design of HEMM achieves an estimated electromagnetic specific power of 17.28 kW/kg at an efficiency of 98.61% (without margins). This estimate is for a rotor coil temperature of 62 K, a rotor coil fill factor of 90%, and a stator winding average temperature of 135 C. In Section VI, the sensitivity of the design to these variables is explored. Electromagnetic losses for the rotor of the updated design are estimated to be ~ 2 W by the efficiency analysis method from Section III. It is likely that this value results from numerical error in the FEA simulations and is not caused by real fluctuations in the magnetic field in the rotor components.

VI.   Sensitivity of Design to Key Variables

At this stage in the design process, a number of uncertainties exist within the design that will not be fully addressed until final manufacturing, assembly, and/or testing of the machine. They include the stator winding's average temperature, the rotor coil's temperature, and the rotor coil's turn count. Risk reduction activities are currently under way to reduce the uncertainty in these variables [8]. The following sections show the sensitivity of the HEMM electromagnetic design to these variables.

A. Effect of Stator Winding Temperature

The average temperature of the stator winding in the actual motor may differ from the 135 C value assumed in the design due to inaccuracies in the thermal design, loss predictions, or errors in manufacturing of the machine. The current stator thermal design and predicted performance is discussed in [9]. At the system level there is also a trade space between stator winding temp and the temperature and flow velocity of the liquid coolant. The required temperature and flow velocity of the coolant will directly relate to the sizing of the thermal management system for an aircraft. The two plots below show the sensitivity of the design to stator winding temperature in terms of efficiency and resistive losses.

Figure 8 Efficiency Variation with Stator Winding Average Temperature
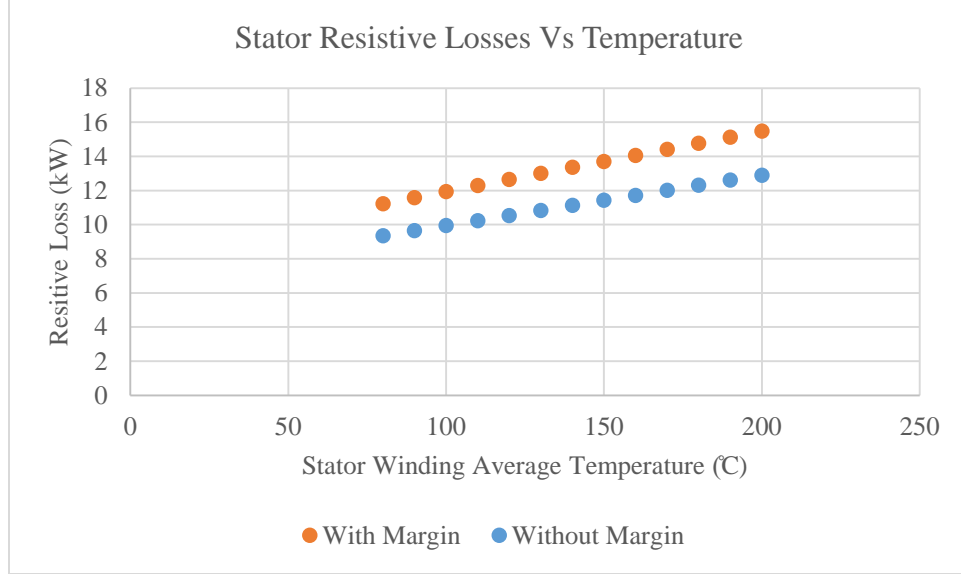
Figure 9 Stator Winding Resistive Loss Variation with Average Stator Winding Temperature

From the above plots trades can be made at the vehicle level in regards to the thermal management system design and the motor winding temperature at the vehicle level. The key take away from the plot in Figure 8 is that the current motor design is able to maintain greater than 98% efficiency up to an average winding temperature of 200 C.

B. Effect of Rotor Coil Layer Turn Count and Temperature

The exact rotor coil turn count that will be achieved in manufacturing as well as the actual temperature the coil will be at in actual motor operation has uncertainty at this point in the design process. Both of these variables directly affect the net magnetic field that the rotor can produce and therefore also the required stator current, stator winding resistive losses, and the stator iron losses.

Rotor coil temperature uncertainty exist at the moment due to the uncertainty in actual cryocooler design/performance [10], the thermal contacts in the machine, and exact losses in rotor. The 62 K design point for HEMM has margin built into it for all three of these uncertainties. Without these margins, the projected rotor coil temperature is near 50 K. Consequently, analysis was carried out on the updated HEMM design between 50 K and 66 K to project machine efficiency across all possible rotor temperatures.

Rotor coil turn count uncertainty mostly results from the tolerance on the superconducting tape and uncertainty in the actual coil fill factor that will be achieved in manufacturing. The superconducting tape used in this motor design has a thickness tolerance of +/- 10 μm on its nominal thickness of 65 μm and the coils are conservatively assumed to have a 90% fill percentage in the nominal design (150 coil layer turns). The possible actual turn counts for a given coil layer therefore range from 130 turns to 197 turns. 130 turns corresponds to a coil with a 75 μm thick superconducting tape and a 90% fill. 197 turns corresponds to a coil with 55 μm thick superconducting tape and 96% fill. The actual turn counts in each of the 48 coil layers of the design will not be known until coil layer winding is completed. To assess the potential impact of this variation in coil layer turns, efficiency analysis was run for coil turn counts of 130, 160, and 190 turns.

For each combination of turn count and rotor coil temperature explored in this section, static simulations were used to determine the critical current in the superconducting tape as well as the required stator current to achieve the target power of the machine. Efficiency analysis was then run as described in Section III for selected cases with rotor coil turn count, coil critical current, and stator current set appropriately for each case. Figures 8 and 9 shows the variation of rotor critical current and stator current for all combinations of coil layer turns and rotor coil temperature.
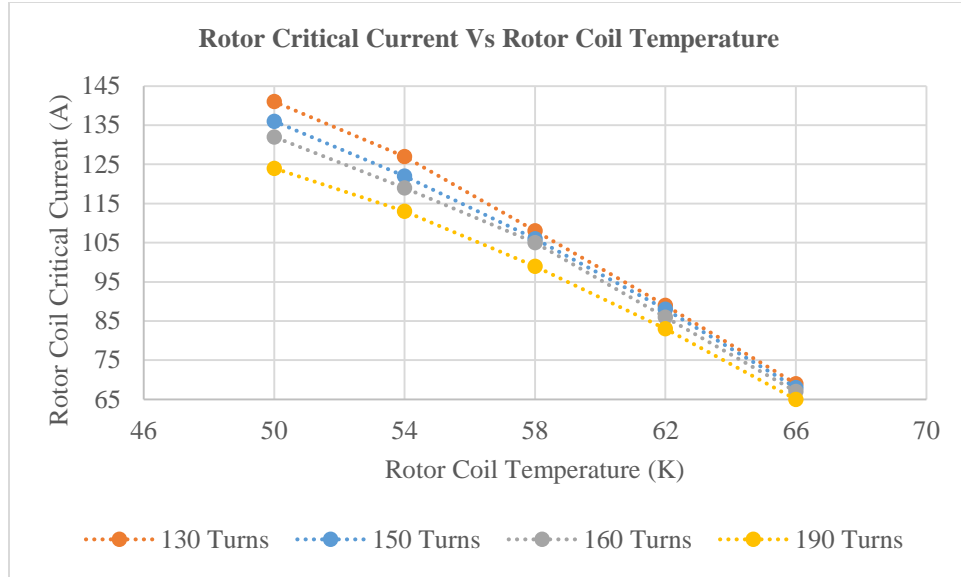
Figure 10 Rotor Critical Current Vs Rotor Coil Temperature and Coil Layer Turns
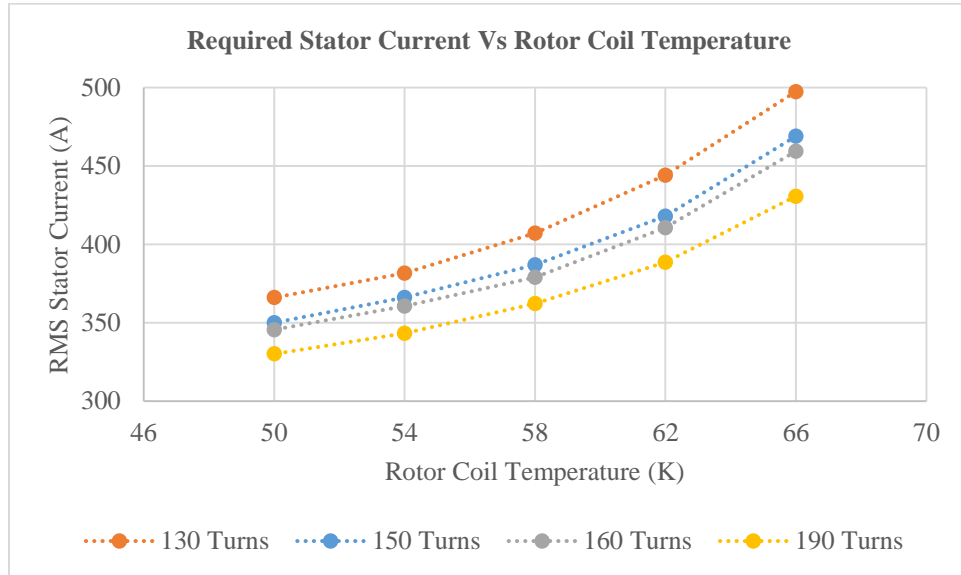

Figure 11 Required Stator Current Vs Rotor Coil Temperature and Coil Layer Turns

In Figure 10, rotor critical current is shown to increase with reduced rotor temperature and turn count as would be expected. Critical current decays with increased coil layer turns because the larger turn count results in a higher peak magnetic field in the conductors at a given rotor current. The reduction in critical current with increased turns is more severe at lower coil temperatures for two reasons. The primary reason is that for a given temperature-induced increase in rotor current, a stronger coil with more turns produces a larger increase in magnetic field. The secondary reason is that at a given magnetic field, the superconductor becomes somewhat more sensitive to the magnetic field as temperature decreases. It is important to note that while critical current is reported in Figure 10, the actual operating current for all the cases run in this section is 65% of that critical current value. Every stator current and efficiency analysis was determined for the operating rotor current not the critical current.

In Figure 11, required stator current decays with decreased rotor coil temperature and increased rotor coil turn count due to the stronger magnetic field produced by the rotor. Diminishing marginal returns are seen as rotor coil temperature reduces; however, because saturation of the rotor and stator iron results in less of the increased magnetic field reaching the full stator coils.

Full efficiency analysis was only carried out for all rotor coil temperatures at the nominal number of turns per coil layer (150) and for all turn counts at 62 K. Figure 12 shows the variation in efficiency with rotor coil temperature at the nominal rotor coil layer turn count of 150 Turns. Figure 13 shows the variation in efficiency with rotor coil layer turn count at the nominal rotor coil temperature of 62 K.
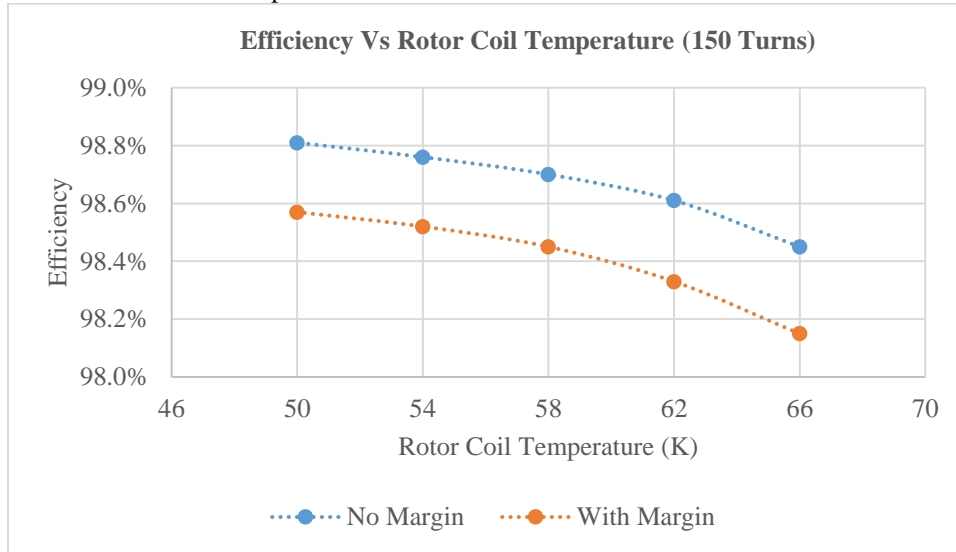
Efficiency Vs Rotor Coil Temperature (150 Turns)

Figure 12 Effect of Rotor Coil Temperature on the Efficiency of HEMM at 150 Coil Layer Turns

As would be expected, machine efficiency is shown to improve with reduced rotor coil temperature in Figure 12. This efficiency improvement is mostly driven by the reduction in required stator current (Figure 11) and it trends with the reduced marginal returns on stator current with reduced rotor coil temperature. Iron losses do increase with the increased magnetic field produced by the rotor as rotor temperature decreases; however, the increase in iron losses due to rotor coil temperature reduction from 66 K to 50 K is only ~1 kW while the reduction in stator resistive losses is ~5kW. Overall, Figure 12 shows that HEMM has a possible efficiency up to 98.8%, but the design can also meet the 98% efficiency target efficiency up to a rotor temperature of 66 K with a 20% loss margin.
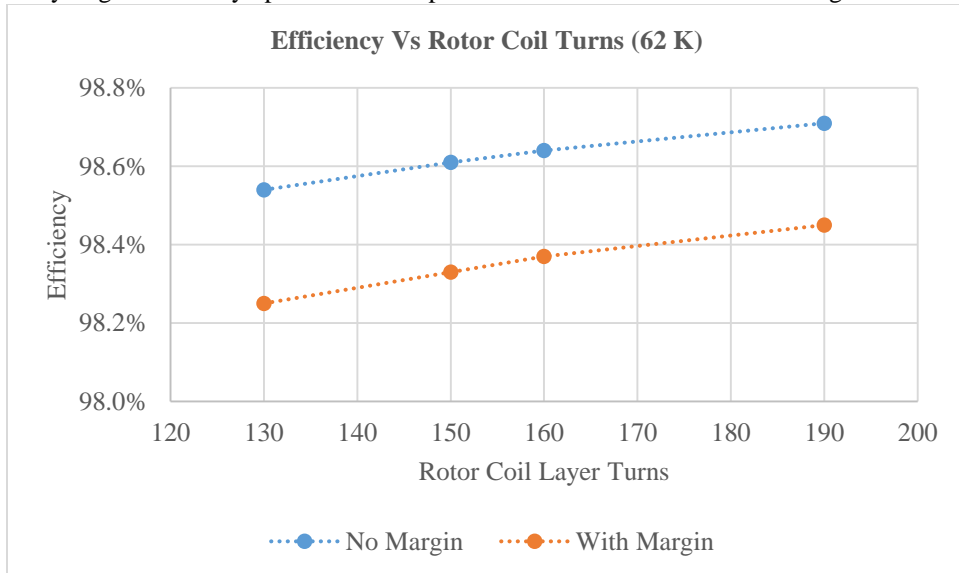
Efficiency Vs Rotor Coil Turns (62 K)

Figure 13 Effect of Rotor Layer Turn Counts on Efficiency at a Rotor Coil Temperature of 62K

In Figure 13, efficiency is shown to improve with increased turn count. This again mirrors the reductions in required stator current with increased coil turn counts in Figure 11. The design is relatively insensitive to rotor coil layer turn count as a reduction in coil turns from 190 to 130 (a 30% reduction) only results in an efficiency reduction

of ~0.2%. Even at the minimum possible turn count of 130 turns the updated HEMM design is shown to be able to achieve the target machine efficiency of 98% in Figure 13.

VII. Conclusion

NASA's High Efficiency Megawatt Motor (HEMM) is a 1.4 MW machine under development at NASA Glenn Research Center targeted at achieving 16 kw/kg electromagnetic power density and 98% efficiency. This paper presented an update to the electromagnetic design of HEMM based on an identified fatal flaw in the preliminary design. The stator teeth in the preliminary design through two separate efficiency analysis were shown to cause substantial magnetic loss in the rotor components. These losses were significantly greater than the <60 watts that HEMM's rotor embedded cryocooler can reject at its 50 K operating temperature. Simple removal of the stator teeth from the preliminary design would have fixed the rotor loss problem, but at a substantial reduction of efficiency. A highly constrained redesign of the motor without stator teeth was therefore carried out and an updated design capable of achieving 16 kW/kg and >98% efficiency was presented. Risk reduction testing of this machines is still in progress and some key variables of the design are still unknown. To that end, the sensitivity of the design to these variables is presented to show that the machine will be able to achieve the target performance regardless of the values of these variables. The sensitivity analysis also shows the potential for the design to achieve much higher efficiency than 98% if certain variables achieve there ideal values. At the time of this papers publication the design is progressing towards CDR. Further tweaks to the electromagnetic design of the machine may occur as a result of risk reduction testing and reviews. The expected completion date for the motor is in 2021.

VIII. Acknowledgments

IX. References

[1] J. R. Welstead and J. L. Flder, "Coceptual Design of a Single-Aisle Tuboelectric Commercial Transport with Fuselage Boundary Layer Ingestion," in *AIAA SciTech 2016*, San Diego, 2016.

[2] R. H. Jansen, Y. De Jesus-Arce, P. Kascak, R. Dyson, A. Woodworth, J. J. Sheidler, R. Edwards, E. Stalcup, J. Whilhite, K. Duffy, P. Passe and S. McCormick, "High Efficiency Megawatt Motor Conceptual Design," in *AIAA Propulsion and Energy Forum*, Cincinnati, 2018.

[3] R. H. Jansen, P. Kascak, R. Dyson, A. Woodworth, J. Scheidler, A. D. Smith, T. Tallerico, Y. De Jesus-Arce, D. Avanesian, K. Duffy, P. Passe and G. Szpak, "High Efficiency Megawatt Motor Prelominary Design," in *AIAA/IEEE Electric Aircraft Technologies Synmposium*, Indianapolis, 2019.

[4] J. J. Scheidler, "Preliminary Design of the Superconducting Rotor for NASA's High-Efficiency Megawatt Motor," in *AIAA Propulsion and Energy Forum*, Cincinnati, 2018.

[5] J. J. Sheidler, T. F. Tallerico, W. A. Miller and W. Torres, "Progress Toward the Critical Design of the Superconducting Rotor for NASA's 1.3 MW High-Efficiency Electric Machine," in *AIAA/IEEE Electric Aircraft Technologies Symposium*, Indianapolis, 2019.

[6] V. Venkatachalam, C. Sullivan, T. Abdallah and H. Tacca, "Accurate Predicition of Ferritie Core Loss with Non-Sinusoidal Waveforms Using only Steinmets Parameters," in *Computers in Power Electronics* , Mayaguez, 2002.

[7] S. Rouho, T. Santa-Norkki, J. Kolehmainen and A. Arkkio, "Modeling Magnet Length in 2-D Finite Element Analysis of Electric Machnines," *IEE Transactions on Magnetics,* vol. 45, no. 8, 2009.

[8] R. H. Jansen, J. Scheidler, T. Tallerico, P. Kascak, A. Woodworth, A. Smith, R. Dyson, W. Sixel, J. Thompson, E. Stalcup, Y. De Jesus-Acre, D. Avanesian, K. Duffy, P. Passe and G. Szpak, "High Efficiency Megawatt Motor Risk Reduction Activities," in *Electrified Aircraft Technologies Symposium*, New Orleans, 2020.

[9] G. Sapak, A. Smith, J. T. Thompson, A. Woodworth and R. Jansen, "High Efficiency Megawatt Motor Thermal Stator Preliminary Design," in *AIAA/IEEE Electrified Aircraft Technologies Symposium*, New Orleans, 2020.

[10] K. P. Duffy, P. J. Passe, R. W. Dyson and R. H. Jansen, "Design Analysis and Testing of the HEMM Cryocooler Linear Motor," in *AIAA/IEEE Electrified Aircraft Technologies Symposium*, New Orleans, 2020.

[11] J. J. Scheidler and T. F. Tallerico, "Design, Fabrication, and Critical Current Testing of No-Insulation Superconducting Rotor Coils for NASA's 1.4 MW High-Efficiency Megawatt Motor," in *AIAA/IEEE Electric Aircraft Technologies Symposium*, Cincinnati, 2018.

[12] R. H. Jansen, G. V. Brown, J. L. Felder and K. P. Duffy, "Turboelectric Aircraft Drive Key Performance Parameters and Functional Requirments," in *AIAA Propusion and Energy Forum*, Orlando, 2015.

[13] A. A. Woodworth, A. Smith, W. Sixel, R. Edwards, R. Jansen, S. McCormick, M. Robbie, G. Szpak, P. Naghipour and E.-S. Shin, "Thermal Analysis of Potted Litz Wire for High-Power-Density Aerospace Electric Machines," in *AIAA Propulsion and Energy Forum*, Indianapolis, 2019.

[14] R. W. Dyson, R. H. Jansen, K. P. Duffy and P. J. Passe, "High Efficiency Megawatt Machine Rotating Cryocooler Conceptual Design," in *AIAA Propulsion and Energy Forum*, Indianapolis, 2019.

[15] M. T. Kakhki, J. Cros and P. Viarouge, "New Approach for Accurate Prediction of Eddy Current Losses in Laminated Material in the Presence of Skin Effect with 2-D FEA," *IEEE Transactions on Magnetics,* vol. 52, no. 3, 2016.